



# Importance of electron-phonon coupling in thermal transport in metal/semiconductor multilayer films

Wuli Miao, Moran Wang\*

Key Laboratory for Thermal Science and Power Engineering of Ministry of Education, Department of Engineering Mechanics and Center for Flexible Electronics Technology, Tsinghua University, N809 Mengminwei Building, Qinghua Yuan, Beijing 100084, China

## ARTICLE INFO

### Article history:

Received 26 April 2022

Revised 21 August 2022

Accepted 11 October 2022

### Keywords:

Thermal conductivity  
Electron-phonon coupling transport  
Metal/semiconductor interface  
Multilayer thin films  
Boltzmann transport equation

## ABSTRACT

Thermal transport across the interface between metals and semiconductors is ubiquitous in micro- and nano-manufacturing devices. The direct simulation of thermal transport in such multilayers is rarely studied due to different main carriers involved, such as electrons in metals and phonons in semiconductors. This study investigates thermal transport in metal/semiconductor multilayer films using the coupled electron and phonon Boltzmann transport equations combined with the phonon diffuse mismatch model. The calculated overall thermal conductivity demonstrates the importance of electron-phonon coupling transport and then the present work gives a critical thickness of the metal layer for considering electron-phonon coupling transport. If only one side of the metal layer is in contact with the semiconductor, the electron-phonon coupling transport in metal layer should be considered when the metal layer thickness is larger than 12.5 nm, 7.5 nm and 2 nm for Au/Si, Cu/Si and Al/Si bilayer films, respectively. This critical thickness will be approximately double if two sides of the metal layer are both in contact with the semiconductor due to the non-equilibrium between electrons and phonons at both sides, such as the super-lattice with infinity periods. Additionally, there exist a minimum thermal conductivity in metal/semiconductor multilayers when changing the thickness of the metal layer. This work will promote a deeper understanding of the thermal transport in metal/semiconductor multilayers at the micro and nanoscale and provide the insightful indication for the manipulation of thermal conductivity in multilayers.

© 2022 Elsevier Ltd. All rights reserved.

## 1. Introduction

Interfaces between metals and semiconductors widely exist in electronic devices and thermoelectric conversion facilities, such as the mutual contact of metallic interconnects and semiconductor parts [1–5]. Introduction of metallic films into thermoelectric super-lattices has improved the figure of merit [6,7]. The thermal transport mechanism across such interfaces between metals and semiconductors becomes increasingly important with the continued miniaturization of devices and facilities [8]. As metals and semiconductors are involved with different main carriers, electrons in metals, and phonons in semiconductors, the energy transfer near the interface introduces an additional thermal resistance, as demonstrated by Majumdar and Reddy [9]. Since the classical Fourier law may not be valid at the micro and nanoscale [8,10,11], a further understanding of heat transport across such interfaces between metals and semiconductors is necessary.

Two transfer channels exist at the interface between metals and semiconductors: (i) electrons in metals coupling with phonons in semiconductors; and (ii) phonons in metals coupling with phonons in semiconductors [12,13]. The contribution of the former is still not clear although quite a few efforts have been paid to give a theoretical modeling of the process [14–20]. The latter contains elastic scattering at the interfaces described by the acoustic mismatch model (AMM) [21] or the diffuse mismatch model (DMM) [22], and the inelastic scattering for which there is no any valid theory yet [23–25]. The AMM, based on the wave picture of phonons, is usually valid at very low temperature [21]. The DMM treats phonons as particles and give an overall good prediction of the thermal boundary conductance at elevated temperature, such as around the room temperature mostly concerned [22]. For interfaces with similar phonon spectra, such as the Al(Co, Ru)/Al<sub>2</sub>O<sub>3</sub> and TiSi<sub>2</sub>(NiSi)/Si interfaces, the measured thermal boundary conductance generally agrees with that predicted by DMM [26–28]. In contrast, DMM underestimates the measured thermal boundary conductance for the Au(Pb)/diamond interfaces between highly dissimilar materials [14,15]. Most literature focuses on the interface conductance by experimental measurement or theoretical analy-

\* Corresponding author.

E-mail address: [mrwang@tsinghua.edu.cn](mailto:mrwang@tsinghua.edu.cn) (M. Wang).

sis, while the temperature distribution and heat flux in multilayer films is rarely discussed [12,26,29,30]. As a first step in investigating the thermal transport in metal/semiconductor multilayer films, material pairs with similar spectra for which the phonon DMM gave a good explanation are selected for this study [27]. In the previous work, phonon conduction was simulated for hybrid organic-inorganic super-lattices or most heterojunctions such as Si/Ge or GaN/AlN constituted by both semiconductors [31–34]. Yet, it is not available directly to the present cases. As electrons are the main heat carriers in metals, the inclusion of electrons is indispensable for the thermal transport in the metal/semiconductor multilayers. Electrons, carrying heat in metals, transfer energy to phonons through electron-phonon (e-ph) coupling near the interface, followed by the phonon transmission or reflection at the interface and phonon transport in semiconductors, actuating thermal transport in multilayers. Thus, simulations of e-ph coupling transport in metal are essential in metal/semiconductor multilayers. This study investigates the thermal transport in such multilayer films and calculates its overall thermal conductivity based on the direct simulation of electron and phonon thermal transport simultaneously.

Majumdar and Reddy first combined the two-temperature model (TTM) in metals and phonon conduction in semiconductors to describe the heat transport across the metal/semiconductor bilayer in 2004 [9]. Later, the extension of TTM, such as the electron and phonon diffusion equations solved by the discrete methods [35] or phonon diffusion modeled by molecular dynamics [36,37], was simulated. Yet, these models may not be suitable at the micro and nanoscale due to either limitations of their macroscopic picture or the failure of incorporating electron thermal transport by molecular dynamics. In comparison, the Boltzmann transport equations (BTEs) provide another avenue by simultaneously considering electron and phonon transport. However, the coupled electron and phonon scattering terms in integral form make the direct solution of BTEs quite challenging [38–41]. Additionally, the drift terms, indispensable for transport issues, are usually neglected for simplicity [38,39,41]. Our previous work proposes a more straightforward treatment of the coupled electron and phonon scattering terms in the form of a relaxation time approximation [42]. Thus, the drift terms can be solved simultaneously. Therefore, we adopt this treatment in the present work. Combined with the phonon DMM description for the interface, this work studies the thermal transport in metal/semiconductor multilayer films using the coupled electron and phonon BTEs. The remaining of this article is organized as follows. In Section 2, a brief introduction of the coupled electron and phonon BTEs and phonon DMM is shown. This transport framework is further validated by comparing the thermal conductivity of multilayer films with experimental measurements. In Section 3, we firstly compare the electron and phonon Knudsen number in metals and then calculate the temperature, heat flux distribution and thermal conductivity in bilayer films then multilayer films. Besides, through comparing the thermal conductivity between with and without e-ph coupling transport, we give a critical thickness of the metal layer. If the metal thickness is larger than this critical thickness, the e-ph coupling transport in metal should be considered. Furthermore, the present work also calculates the thermal conductivity under keeping the total thickness constant and changing the metal layer thickness. The concluding remarks are finally made in Section 4.

## 2. Mathematical model

The schematic of the thermal transport in bilayer films is shown in Fig. 1. The electron, phonon coupling transport is simulated in metal, and the phonon transport is considered in semiconductor, with the interfacial condition described by DMM.

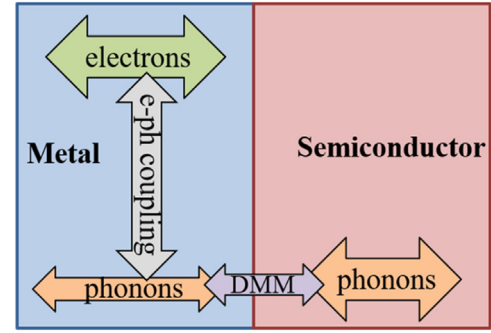


**Fig. 1.** Schematic of thermal transport in metal/semiconductor bilayer films. The electron, phonon coupling transport is simulated in metal, and the phonon transport is considered in semiconductor, with the interfacial condition described by DMM.

The intensity form of the coupled electron and phonon BTEs in metal is formulated as [42]

$$\frac{\partial I_\varepsilon}{\partial t} + \mathbf{v}_\varepsilon \cdot \nabla_{\mathbf{r}} I_\varepsilon = -\frac{I_\varepsilon - I_\varepsilon^{eq}(\tilde{T}_e)}{\tau_{e-ph}(\varepsilon)} \quad (1)$$

$$\frac{\partial \phi_{\omega,p}}{\partial t} + \mathbf{v}_{ph,p}^m \cdot \nabla_{\mathbf{r}} \phi_{\omega,p} = -\frac{\phi_{\omega,p} - \phi_{\omega,p}^{eq}(\tilde{T}_e)}{\tau_{ph-e}(\omega, p)} - \frac{\phi_{\omega,p} - \phi_{\omega,p}^{eq}(\tilde{T}_{ph,m})}{\tau_{U,ph-ph}} \quad (2)$$

where,  $I_\varepsilon$  and  $\phi_{\omega,p}$  are the electron and phonon intensity in metal, respectively,  $\varepsilon$  the electron energy,  $\omega$  the phonon frequency and  $p$  the different branches including the transverse acoustic (TA) and longitudinal acoustic (LA) phonons. For simplicity, we use the abbreviation  $m$  to denote metal. The electron-electron interaction is neglected in formulating the scattering term of electrons due to both the screen effect and the Pauli exclusion principle [43].  $\tilde{T}_{ph,m}$  and  $\tilde{T}_e$  are the local pseudo-temperatures of phonons and electrons, respectively, in the metal determined by the energy conservation principle during the phonon-phonon (ph-ph) collision and the e-ph collision processes separately.

The energy-dependent e-ph relaxation time  $\tau_{e-ph}(\varepsilon)$  in Eq. (1), the frequency-dependent ph-e relaxation time  $\tau_{ph-e}(\omega, p)$ , and the ph-ph Umklapp relaxation time in Eq. (2) are from reference [42]. The free electron band structure and the power law approximation of the isotropic phonon dispersion relation along the [0 0 1] direction are used for the metal; the detailed parameters are also found in Ref. [42].

First, we consider the intrinsic semiconductor, so phonon transport is simulated without considering electron or hole transport. Thus, the intensity form of phonon BTE in a semiconductor is

$$\frac{\partial \varphi_{\omega,p}}{\partial t} + \mathbf{v}_{ph,p}^s \cdot \nabla_{\mathbf{r}} \varphi_{\omega,p} = -\frac{\varphi_{\omega,p} - \varphi_{\omega,p}^{eq}(\tilde{T}_{ph,s})}{\tau_s(\omega, p)}, \quad (3)$$

where,  $\varphi_{\omega,p}$  denotes phonon intensity. The abbreviation  $s$  represents semiconductor, to distinguish with metal in Eq. (2).  $\tilde{T}_{ph,s}$  is the local pseudo-temperature of phonons in semiconductor determined by the energy conservation principle during the phonon scattering process.  $\tau_s(\omega, p)$  is the phonon relaxation time in semiconductor including Umklapp scattering and impurity scattering; the detailed expression can be found in Ref. [33]. The power law approximation of the isotropic phonon dispersion relation along the [0 0 1] direction is adopted for the semiconductor with the detailed parameters also found in Ref. [33].

Electrons in metals are assumed to be adiabatic at the interface from metal to semiconductor and not transmitted due to the barrier [9]. DMM describes the phonon interfacial condition with the

spectral transmission coefficient  $\alpha_{m-s}$  from metal to semiconductor and  $\alpha_{s-m}$  from semiconductor to metal expressed as [33]

$$\alpha_{m-s}(\omega, \mathbf{p}) = \frac{[k_{s,p}(\omega)]^2}{[k_{m,p}(\omega)]^2 + [k_{s,p}(\omega)]^2}, \quad (4)$$

$$\alpha_{s-m}(\omega, \mathbf{p}) = \frac{[k_{m,p}(\omega)]^2}{[k_{m,p}(\omega)]^2 + [k_{s,p}(\omega)]^2}. \quad (5)$$

$k_{m,p}(\omega)$  and  $k_{s,p}(\omega)$  are the magnitude of phonon wave vector of metal and semiconductor, respectively.

Once the electron and phonon intensities in metal and phonon intensity in semiconductor are resolved, the local electron and phonon energy density  $E_e(t, \mathbf{r}), E_{ph,m}(t, \mathbf{r})$  and heat flux  $\mathbf{q}_e(t, \mathbf{r}), \mathbf{q}_{ph,m}(t, \mathbf{r})$  in metal, the local phonon energy density  $E_{ph,s}(t, \mathbf{r})$  and heat flux  $\mathbf{q}_{ph,s}(t, \mathbf{r})$  in semiconductor are thus calculated:

$$\begin{aligned} E_e(t, \mathbf{r}) &= \int \int_{4\pi} \frac{I_\varepsilon}{v_e} d\Omega d\varepsilon = \int \int_{4\pi} \frac{I_\varepsilon^{\text{eq}}(T_e)}{v_e} d\Omega d\varepsilon; \\ \mathbf{q}_e(t, \mathbf{r}) &= \int \int_{4\pi} \frac{\mathbf{v}_e I_\varepsilon}{v_e} d\Omega d\varepsilon; \end{aligned} \quad (6)$$

$$\begin{aligned} E_{ph,m}(t, \mathbf{r}) &= \sum_p \int \int_{4\pi} \frac{\phi_{\omega,p}}{v_{ph,p}^m} d\Omega d\omega = \sum_p \int \int_{4\pi} \frac{\phi_{\omega,p}^{\text{eq}}(T_{ph,m})}{v_{ph,p}^m} d\Omega d\omega; \\ \mathbf{q}_{ph,m}(t, \mathbf{r}) &= \sum_p \int \int_{4\pi} \frac{\mathbf{v}_{ph,p}^m \phi_{\omega,p}}{v_{ph,p}^m} d\Omega d\omega; \end{aligned} \quad (7)$$

$$\begin{aligned} E_{ph,s}(t, \mathbf{r}) &= \sum_p \int \int_{4\pi} \frac{\varphi_{\omega,p}}{v_{ph,p}^s} d\Omega d\omega = \sum_p \int \int_{4\pi} \frac{\varphi_{\omega,p}^{\text{eq}}(T_{ph,s})}{v_{ph,p}^s} d\Omega d\omega; \\ \mathbf{q}_{ph,s}(t, \mathbf{r}) &= \sum_p \int \int_{4\pi} \frac{\mathbf{v}_{ph,p}^s \varphi_{\omega,p}}{v_{ph,p}^s} d\Omega d\omega; \end{aligned} \quad (8)$$

where  $\Omega$  is the solid angle. The local temperature  $T_e, T_{ph,m}, T_{ph,s}$  are computed by the inverse integration of the corresponding energy density.

For the numerical solution of the thermal transport across the interface, the discrete-ordinate-method is applied. An implicit and first-order upwind scheme is used for temporal and spatial discretization [42,44]. Additionally, the Gauss-Legendre (G-L) quadrature is adopted for the numerical integration over the phonon frequency, the electron energy, and the angular variable due to its high efficiency [45]. Specifically, due to the mismatch of the phonon spectra between different materials, the discretization of the branch with a higher cut-off frequency is segmented. Thus the common frequency range between the material pairs is identically discretized [45].

The thermal conductivity of the multilayers that includes the influence of the interface and conduction resistances of the constituting films is used to verify the framework shown in Fig. 1, even though the existing experimental data of the thermal conductivity of multilayers is not sufficient as those of the interface conductance [46–49]. One experiment has shown that the thermal conductivity of Au/Si multilayers composed of 10 periods, with Au film 5.7 nm and Si film 3.0 nm in each period is  $0.33 \pm 0.04 \text{ Wm}^{-1}\text{K}^{-1}$  at room temperature [49]. We use the method described above to simulate the thermal transport in such Au/Si multilayers. The calculated thermal conductivity is  $0.303 \text{ Wm}^{-1}\text{K}^{-1}$ , which agrees with the experimental measurements. This agreement further validates our framework for simulating the thermal transport across the interface.

### 3. Results and discussion

#### 3.1. Comparison of Knudsen number

First of all, we calculate the electron and phonon mean free path in metal and compare the corresponding Knudsen number. The electron, phonon mean free path depends on the electron energy, phonon spectrum, respectively. If averaging as follows:

$$\Lambda_e = \frac{\int_{\text{Fermi window}} (\varepsilon - \varepsilon_F) \nabla_T f_\varepsilon^{\text{eq}}(T) v_e \tau_{e-ph}(\varepsilon) D_e(\varepsilon) d\varepsilon}{\int_{\text{Fermi window}} (\varepsilon - \varepsilon_F) \nabla_T f_\varepsilon^{\text{eq}}(T) D_e(\varepsilon) d\varepsilon} \quad (9)$$

$$\Lambda_{ph} = \frac{\sum_p \int_0^{\omega_{\text{max},p}} \hbar \omega \nabla_T n_{\omega,p}^{\text{eq}}(T) v_{ph,p}^m (\tau_{ph-e}^{-1} + \tau_{U,ph-ph}^{-1})^{-1} D_{ph}(\omega, \mathbf{p}) d\omega}{\sum_p \int_0^{\omega_{\text{max},p}} \hbar \omega \nabla_T n_{\omega,p}^{\text{eq}}(T) D_{ph}(\omega, \mathbf{p}) d\omega} \quad (10)$$

The averaged electron and phonon mean free path in metal is obtained.  $f_\varepsilon^{\text{eq}}(T)$  and  $n_{\omega,p}^{\text{eq}}(T)$  are the equilibrium distribution function of electrons and phonons, described by Fermi–Dirac distribution and Bose–Einstein distribution, respectively.  $D_e(\varepsilon)$  and  $D_{ph}(\omega, \mathbf{p})$  are the electron and phonon density of states separately. Fig. 2 shows electron and phonon Knudsen number under different characteristic thickness of the metal layer in Au, Cu and Al. The Knudsen number of electrons is nearly one order of magnitude larger than that of phonons. It means that the scattering of electrons by phonons is not frequent as compared to phonon interaction with itself. Thus, at the interface, it also might be harder for electrons in metal to interact with phonons in semiconductor. Therefore, we neglect this kind of interaction across the interface as a first step, while adopt the phonon DMM to describe phonons in metal coupling with phonons in semiconductor. Overall, based on the following two reasons: (i) For interfaces with similar spectra, for example the ratio of Debye temperature between constituting materials is less than 5 [50], phonon DMM can give a good explanation of the thermal boundary conductance. Although Debye temperature cannot fully represent the spectra, it is still a reference information. For material pairs studied in the present work, such as Au/Si, Cu/Si and Al/Si, the Debye temperature ratio is about 3.9, 1.9 and 1.5, respectively, which satisfy the demand of similar spectra. (ii) Compared to phonons in metal, electrons are not frequently scattered and are harder to couple with phonons in semiconductor. The comparison of Knudsen number further demonstrates that neglecting the coupling between electrons in metal and phonons in semiconductor is kind of proper. Therefore, the present work adopts phonon interaction across the interface by DMM as a first step.

#### 3.2. Critical thickness of the metal layer for considering e-ph coupling transport

In this sub-section, we will apply the validated framework to study the thermal transport in bilayer films firstly, then multilayer films, including Au/Si, Cu/Si, and Al/Si. The results of Ag/Si are similar to that of Au/Si, and not shown in this work. Through comparing the thermal conductivity between with and without e-ph coupling transport, the critical thickness of the metal layer is obtained for both bilayer and superlattice. If the metal layer thickness is larger than this critical thickness, the e-ph coupling transport in metal should be considered.

##### 3.2.1. Bi-layer films

A one-dimensional simulation across the interface is adopted. The temperature of  $T_h=301 \text{ K}$  and  $T_c=299 \text{ K}$  is assigned on the left boundary of the metal and right boundary of the semiconductor, respectively, and the treatment is shown in Appendix. For

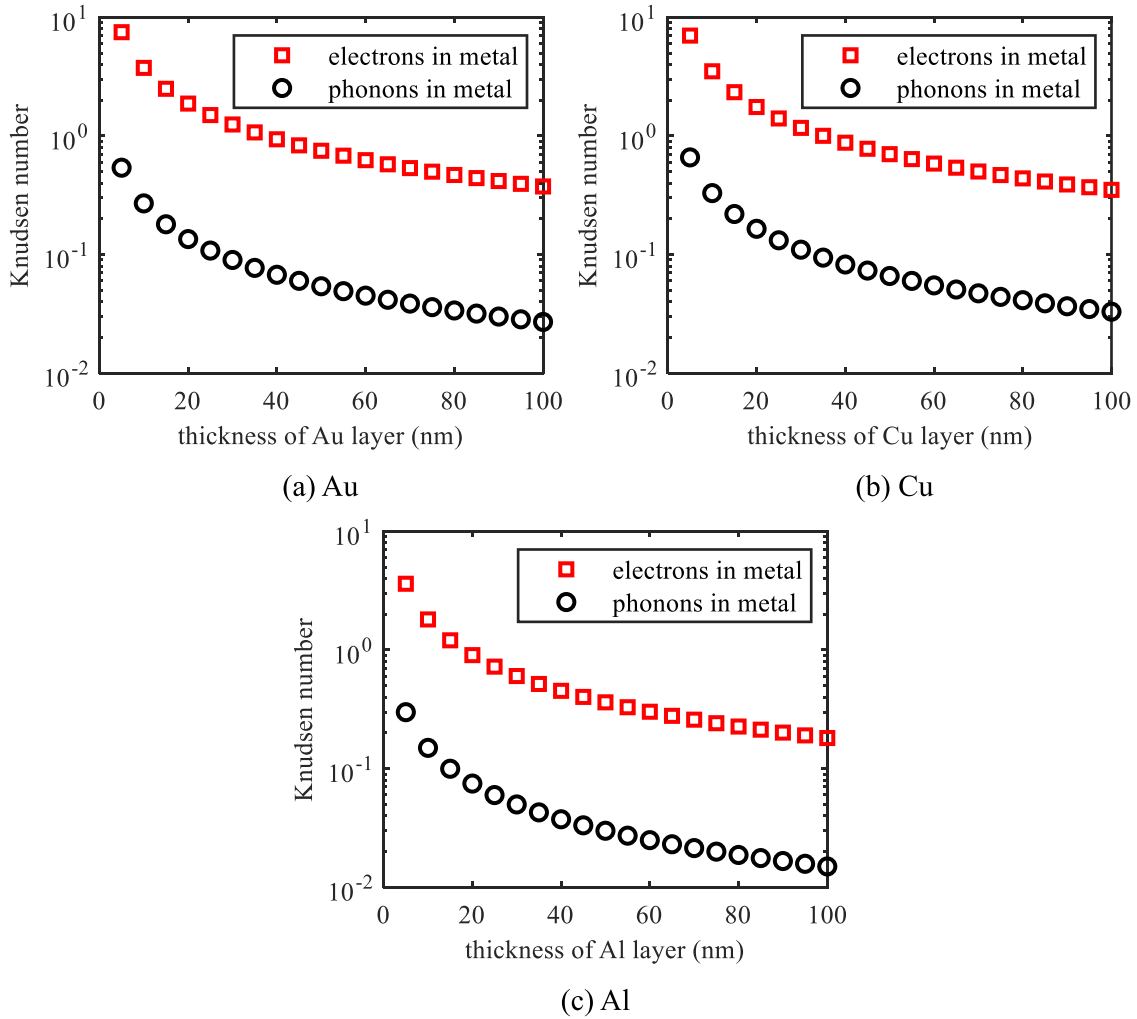


Fig. 2. Electron and phonon Knudsen number under different characteristic thickness of the metal layer.

Table 1

Number of discretization points for phonon spectra for Au/Si, Cu/Si, and Al/Si.

Material pair	TA branch (points/points)	LA branch (points/points)
Au/Si	16/24	24/56
Cu/Si	32/24	40/56
Al/Si	32/24	48/56

the numerical solution of Boltzmann transport equations in intensity form, Eqs. (1)–(3), the present work uses implicit transient scheme. The time step is chosen as 5 fs for Cu/Si and Al/Si, 10 fs for Au/Si. The convergence accuracy is set as  $2 \times 10^{-11}$ . Additionally, the number of abscissas of the G-L quadrature is selected as 48 and 32 points for electron energy and polar angle, respectively. The discretization of the phonon spectra for Au/Si, Cu/Si, and Al/Si is shown in Table 1. Although the number of discretization points for silicon is the same among different material pairs, the detailed discretization is different due to the mismatch of the phonon spectra.

The convergence rate of phonons in metal is slow due to the small mean free path. Correspondingly, the spatial discretization of metal is required to be denser. Thus, the number of spatial grids is 1251 for Al with 10 nm, 2001 for Cu and Au with 10 nm, compared

to 41 for Si with 10 nm. Additionally, for the thickness of 50 nm, Au, Cu, and Al are all discretized with 4001 points, whereas Si is discretized with 201 points. The normalized temperature distribution  $\Theta = (T - T_c)/(T_h - T_c)$  for Au/Si, Cu/Si, and Al/Si is shown in Fig. 3.

At the interface on the metal side, the electrons and phonons display non-equilibrium with different temperatures as shown in Fig. 3. For Au and Cu, with a lower e-ph coupling constant, the weaker strength of energy exchange between electrons and phonons seems more difficult to reach equilibrium. When it approaches the left boundary of the metal, non-equilibrium still exists between electrons and phonons for a metal thickness of 10 nm. Thus, the definition of an effective interface temperature is complex and inconclusive. This interception at the interface is used as an effective interface temperature in the previous work [9,51]. It starts from the equilibrium temperature between electrons and phonons and then linearly extends it to the interface [9,51]. However, it does not apply to the present cases that the thickness of each layer is comparable to the carrier's mean free path. Further, the phonon temperature in metal gradually displays a nonlinear relation due to the energy exchange between electrons and phonons. This nonlinear tendency is more evident for the thicker metal layer, as shown in Fig. 3 (b), (d) and (f). As demonstrated in our previous work, when the metal layer thickness decreases, the energy exchange between electrons and phonons decreases, resulting in

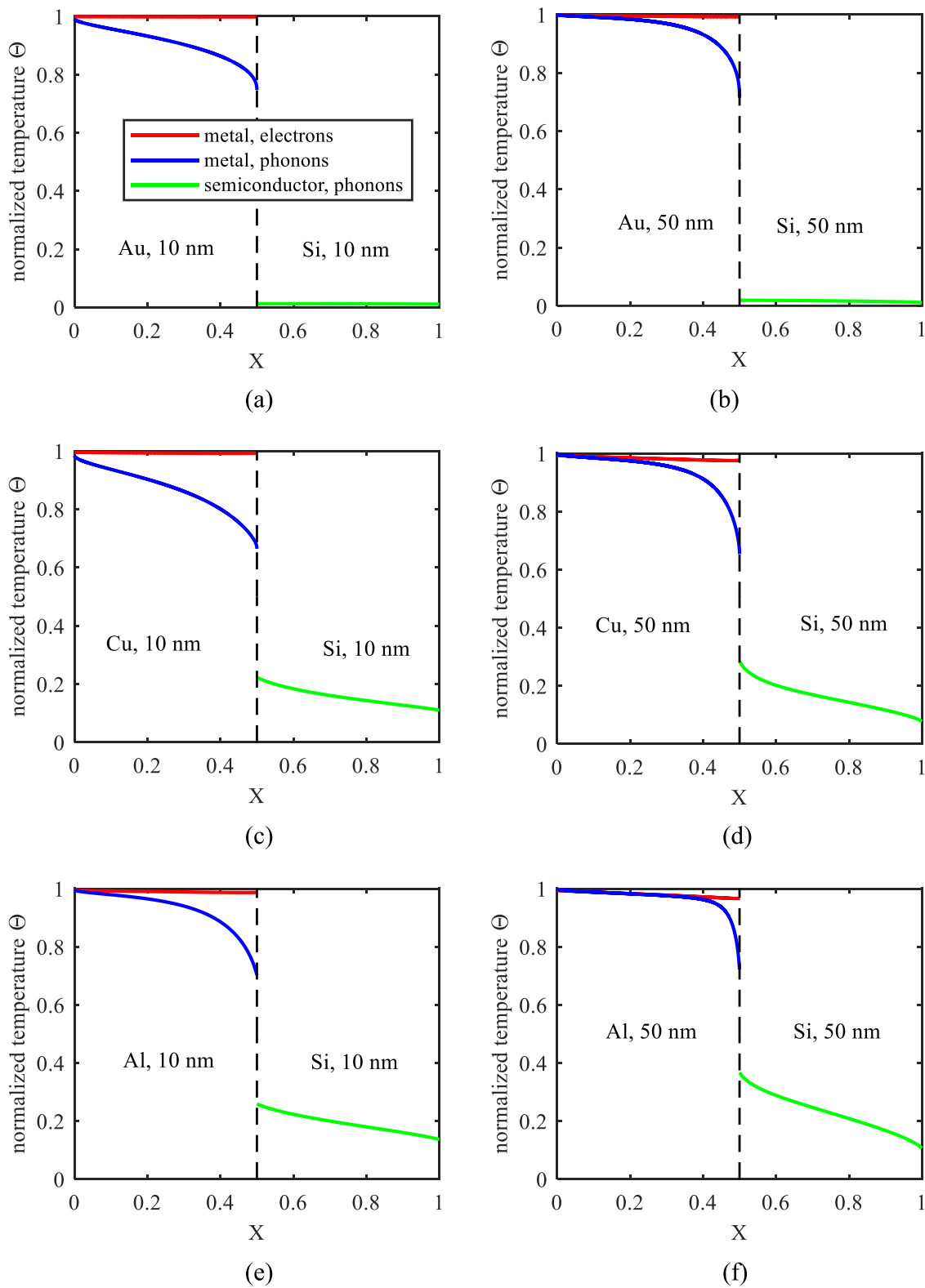


**Fig. 3.** Normalized temperature distribution in metal/semiconductor bilayer films: (a) Au/Si, (c) Cu/Si, (e) Al/Si with the thickness 10 nm of each layer; (b) Au/Si, (d) Cu/Si, (f) Al/Si with the thickness 50 nm of each layer. The red and blue lines denote the electron and phonon temperature in metal, respectively, whereas the green line represents the phonon temperature in the semiconductor. The black dashed line is depicted for the interface.

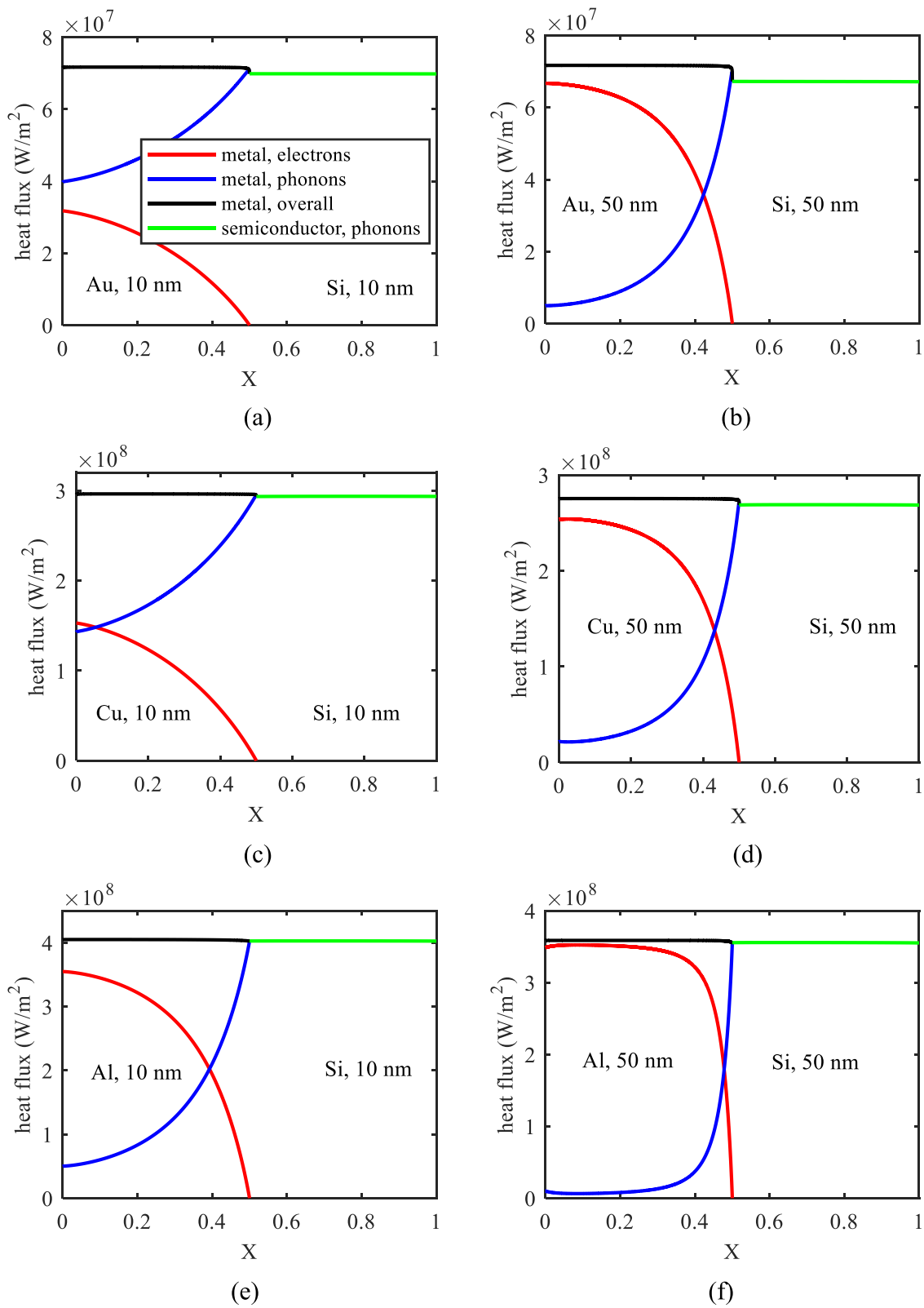


**Fig. 4.** Heat flux distribution in metal/semiconductor bilayer films: (a) Au/Si, (c) Cu/Si, (e) Al/Si with the thickness 10 nm of each layer; (b) Au/Si, (d) Cu/Si, (f) Al/Si with the thickness 50 nm of each layer. The red and blue lines denote the heat flux carried by electrons and phonons in metal, respectively. The black line represents the overall heat flux in metal, whereas the green line shows that in the semiconductor.

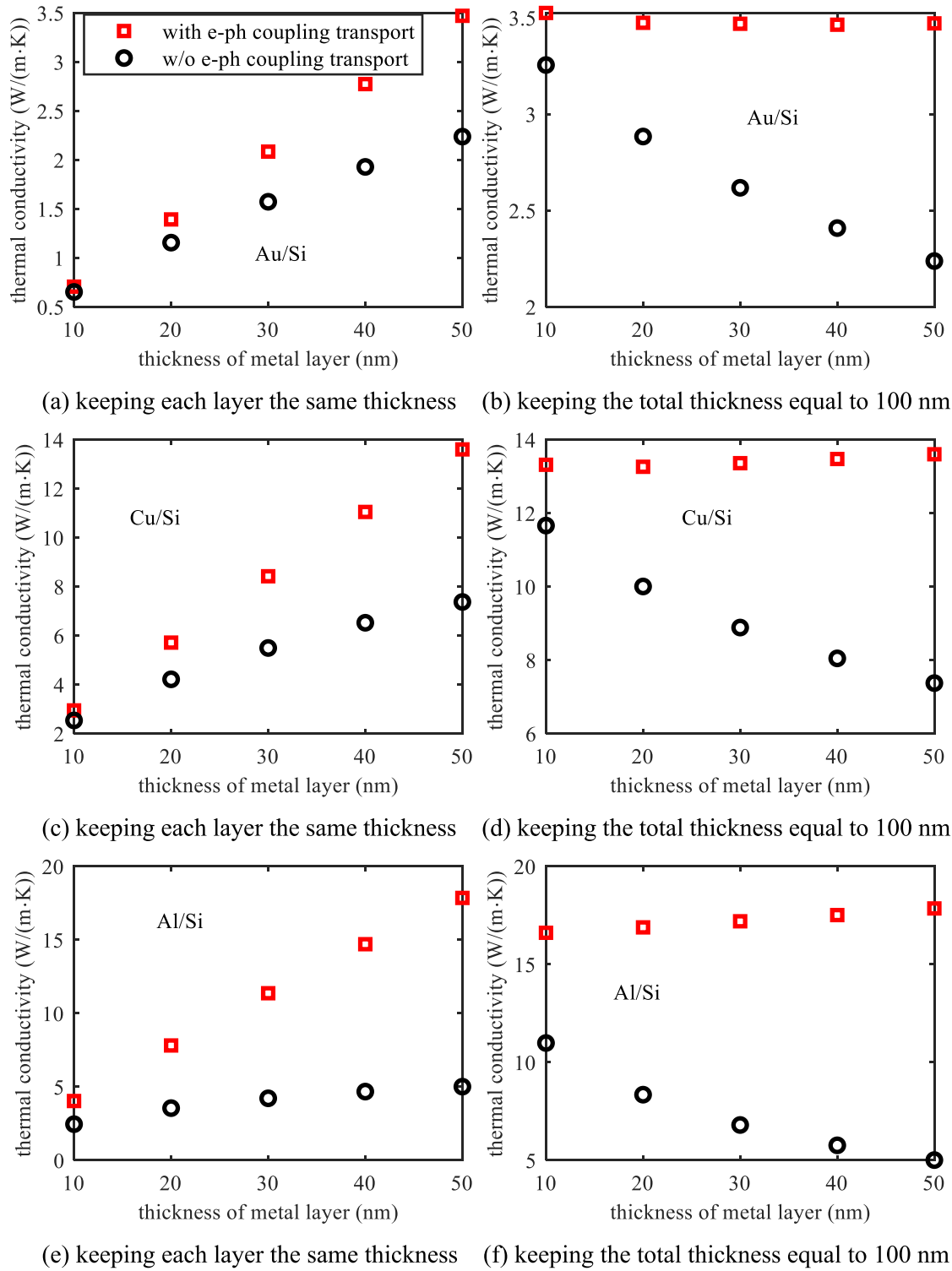


**Fig. 5.** Overall thermal conductivity of metal/semiconductor bilayer films: (a) Au/Si, (c) Cu/Si, (e) Al/Si by keeping each layer the same thickness; (b) Au/Si, (d) Cu/Si, (f) Al/Si by keeping the total thickness equal to 100 nm. The red squares denote the overall thermal conductivity calculated by the present framework, whereas the black circles represent that only simulating phonon transport in metal without consideration of e-ph coupling transport.

this nonlinear tendency also decreasing, as shown in Fig. 3 (a), (c) and (e). Besides, if the e-ph coupling constant in metal is larger, such as Al, this nonlinear tendency is also more obvious.

The heat flux in Fig. 4 clearly shows that electrons carrying heat in metal transfer energy to phonons near the interface through e-ph coupling. Then combined with the phonon transmission or reflection at the interface, the thermal transport across the whole

system is realized. However, the heat flux in the Au/Si bilayer with a thickness of 50 nm each layer is slightly non-conservative due to the high thermal resistance in the system. Therefore, a denser spatial discretization will yield greater conservation. Limited by the computational memory, the current result in Fig. 4 (b) is displayed, and the denser discretization does not influence the result much. Other cases show good convergence. For a large metal layer thick-

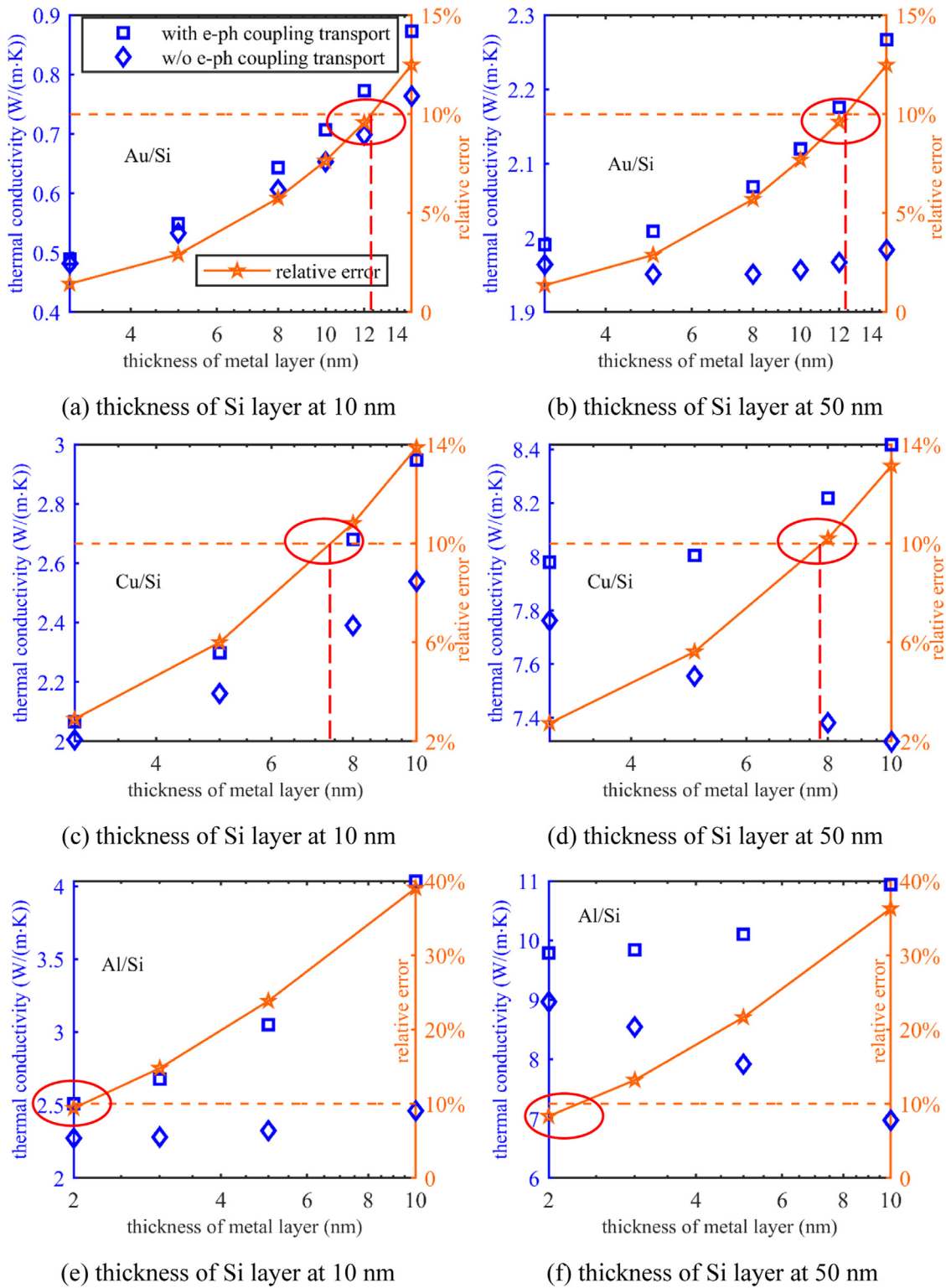


**Fig. 6.** Overall thermal conductivity of metal/semiconductor bilayer films: (a) Au/Si, (c) Cu/Si, (e) Al/Si by keeping thickness of Si layer at 10 nm; (b) Au/Si, (d) Cu/Si, (f) Al/Si by keeping thickness of Si layer at 50 nm. The blue squares and diamonds denote the overall thermal conductivity with and without e-ph coupling transport, respectively. The orange marks represent the relative error between each other.

ness, electrons dominating conduction in a metal carry the majority of the heat and rapidly transfer it to phonons near the interface, as shown in Fig. 4 (b), (d) and (f). In comparison, the dominant role of electrons is weakened for 10 nm thickness due to the insufficient thermalization with the boundary. Thus, the heat carried by phonons in metal is almost numerically equivalent to that carried

by electrons, as shown in Fig. 4 (a) and (c). This weakened role for Al with the largest e-ph coupling constant is not as evident as that for Au, Cu and it will occur if the thickness of Al is small enough. However, if only the phonon conduction without e-ph coupling is considered, the heat flux in the whole system will be significantly underestimated. This is attributed to the notably weak ability of

phonons to conduct heat in metal, i.e., the thermal conductivity of phonons in metal is almost two orders of magnitude smaller than that of electrons.

For a deeper quantitative comparison, the overall thermal conductivity of bilayers is calculated by  $\kappa = q \times L/\Delta T$ , where  $\Delta T$  is the temperature difference across the bilayer, and  $L$  is the total thickness of the bilayer, as shown in Fig. 5.  $q$  is the heat flux denoted by the overall one in metal or the phonon one in semiconductor. In numerical calculation, the averaged value of both is used. The left panel shows the results of keeping each layer the same thickness whereas the right panel shows that of keeping the total thickness equal to 100 nm. The Au/Si bilayers exhibit the smallest thermal conductivity, nearly one order of magnitude smaller than the Cu/Si and Al/Si bilayers, while the thermal conductivity of Al/Si bilayers is the highest. The reasons are as follows. For one thing, the e-ph coupling constant is largest for Al, while the smallest for Au [42]. The larger e-ph coupling constant means stronger energy exchange between electrons and phonons so that more energy transfer can be achieved in Al. For another, the thermal boundary conductance predicted by phonon DMM is the highest for Al/Si interface, while the lowest for Au/Si interface. Thus, for Al/Si, more phonons can be transmitted from semiconductor to metal, and then couple with electrons in metal to achieve energy transfer. Considering the above two aspects, electrons in Al/Si bilayer can carry more heat, thereby showing the lowest resistance. However, the resistance of Au/Si bilayer is the largest, thus the smallest thermal conductivity. For comparison, the results that only simulate the phonon transport in metal without considering e-ph coupling transport are also shown. Generally, these results greatly underestimate the overall thermal conductivity or even predict a wrong trend without e-ph coupling transport. This underestimation will increase as the metal layer thickness increases due to the electrons dominating heat conduction in metal. Furthermore, this underestimation for the Al/Si bilayers is more significant than that for the Au/Si and Cu/Si bilayer. It is attributed to Al having the largest e-ph coupling constant: a stronger ability to exchange energy between electrons and phonons in metal. These demonstrate that the inclusion of e-ph coupling transport in metal is significant for a more complete description of thermal transport in such metal/semiconductor bilayer films.

Noteworthy, if the metal layer is thin enough, the dominant role of electron heat conduction is greatly suppressed. Thus, the thermal conductivity, calculated by neglecting the electron conduction and only considering the phonon conduction in metal, is very close to that considering the e-ph coupling transport in metal. Therefore, there might exist a critical thickness of the metal layer below which the electron heat conduction in metal can be ignored. Fig. 6 demonstrates this point. It shows the obtained thermal conductivity by varying the metal layer thickness when holding the Si film thickness constant at 10 nm and 50 nm, respectively. For comparison, the relative error between with and without e-ph coupling transport is also displayed. Basically, this relative error does not change with the Si film thickness. If we can accept this relative error within 10%, this corresponds to a critical metal layer thickness. When the thickness of Au, Cu and Al layer is larger than this critical thickness, i.e., 12.5 nm, 7.5 nm and 2 nm in Au/Si, Cu/Si and Al/Si bilayer films, the e-ph coupling transport in metal layer should be considered. On the other hand, when the metal layer thickness is smaller than the corresponding critical thickness, the electron heat conduction can be neglected and only phonon conduction can be simulated for convenience. The energy exchange strength between electrons and phonons denoted by e-ph coupling constant is weakest for Au so that the largest thickness is required to show the role of electron heat conduction. Nevertheless, the quantum size effect might be significant at the thin thickness, such as less than 5 nm, which could lead to the change of band struc-

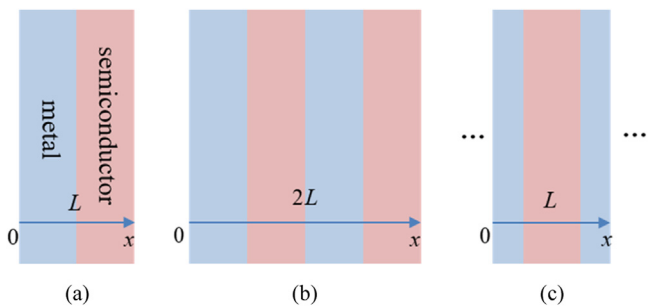


Fig. 7. Schematic of metal/semiconductor multilayer films: (a) one period, isothermal boundary at both sides; (b) two periods, isothermal boundary at both sides; (c) representative structure of super-lattice with infinity periods, periodic heat flux boundary at both sides.

ture and dispersion relation [52,53]. For the metal thickness studied in the present work, most are larger than 5 nm and thus this quantum size effect is not taken into account as a first step.

### 3.2.2. Multi-layer films

In this sub-section, if we treat metal/semiconductor bilayer as one period, we investigate the thermal transport in multilayers with more than one period. Fig. 7 shows the schematic of one period, two periods and infinity periods where  $L$  denotes the thickness of one period. For cases of finite periods, the isothermal boundary conditions are applied whereas the periodic heat flux boundary is used for multilayers with infinity periods.

As for finite periods with isothermal boundary, the temperature of  $T_h=301$  K and  $T_c=299$  K is adopted. The isothermal boundary in the left-most metal layer is assigned on electrons and phonons simultaneously, as shown in Appendix. At the interface, electrons are assumed to be adiabatic whereas phonons are transmitted or reflected, described by DMM. For infinity periods, its representative structure is shown in Fig. 7.(c) and the periodic heat flux boundary is applied at two sides. This boundary condition means the heat flux through the structure is constant. Thus, only the representative structure shown in Fig. 7.(c) needs to be simulated, then realizing the simulation of super-lattice with infinity periods. The formulation of periodic heat flux boundary is displayed in Appendix.

The normalized temperature and heat flux distribution in multilayer films including two periods and representative structure of super-lattice are displayed in Figs. 8 and 9, respectively. For multilayers with two periods, both sides of the middle metal layer are in contact with semiconductor, compared to only one side in contact with semiconductor for the left-most metal layer. Thus, non-equilibrium between electrons and phonons exists at two sides, as shown in Fig. 8.(a)  $X \in [0.5, 0.75]$ , so that the heat flux carried by electrons is also further suppressed, as displayed in Fig. 9.(a)  $X \in [0.5, 0.75]$ . Due to the non-equilibrium at both sides, the energy exchange process between electrons and phonons happens twice: one is from phonons to electrons, the other is from electrons to phonons. From one side of the metal layer, phonons transmitted from semiconductors or reflected by the interface in metals transfer energy to electrons through e-ph scattering. Afterwards, electrons that obtain energy, transport in the metal layer, and then transfer energy to phonons when about to reach the other side of the metal layer. Thus, the heat flux carried by electrons first increases and then decreases, as shown in Fig. 9.(a)  $X \in [0.5, 0.75]$ . In comparison, for the left-most metal layer, only one side contacts with semiconductor and the energy transfer is from electrons to phonons. When the thickness of this metal layer is comparable to the mean free path of electrons by e-ph scattering, a certain amount of energy exchange between electrons and phonons can be realized. However, for the middle metal layer in contact with

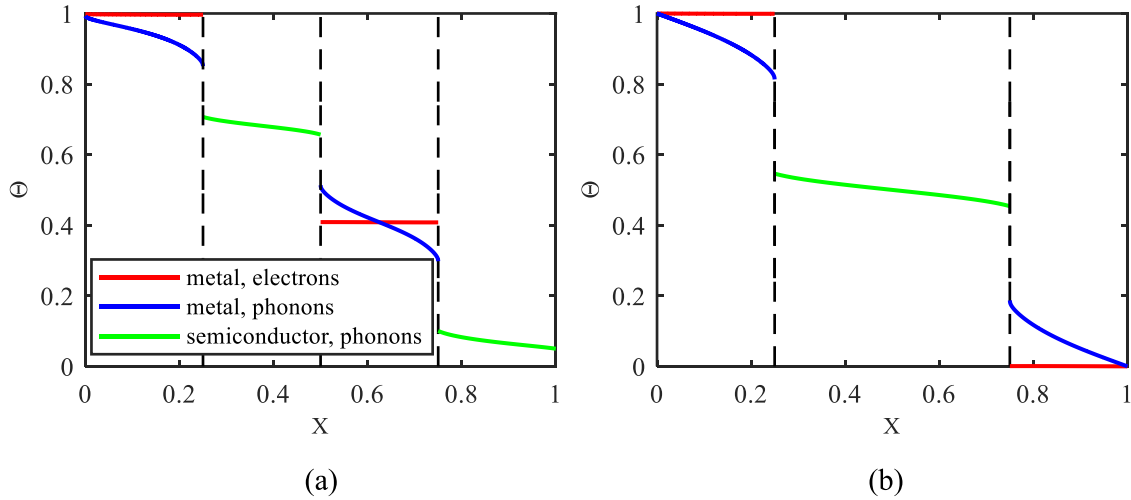


**Fig. 8.** Normalized temperature distribution  $\Theta = (T - T_c)/(T_h - T_c)$  in Cu/Si multilayer films, thickness of one period  $L = 20$  nm with Si and Cu layer both 10 nm: (a) two periods,  $X = x/2L$ ; (b) representative structure of superlattice with infinity periods,  $X = x/L$ .

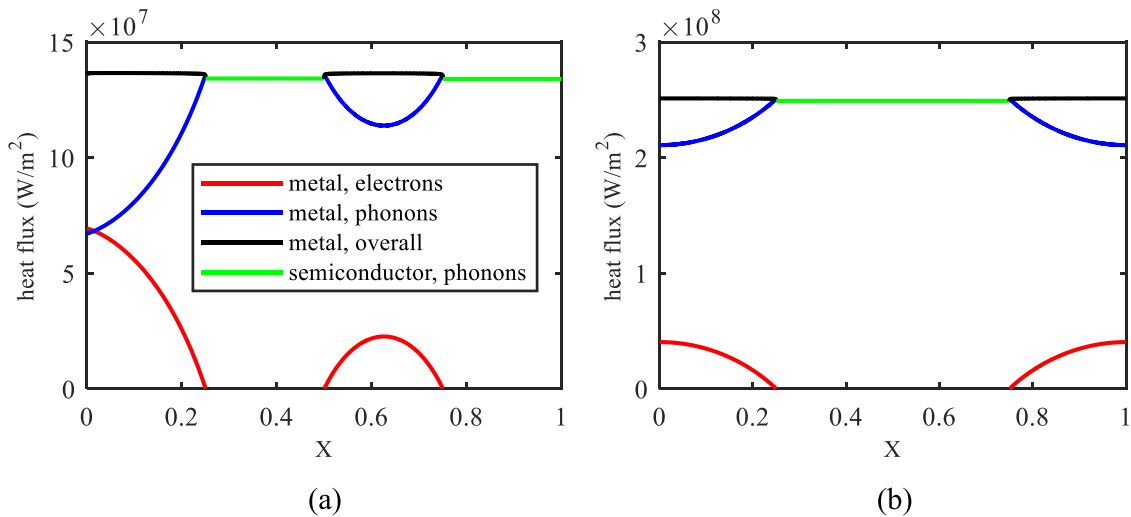


**Fig. 9.** Heat flux distribution in Cu/Si multilayer films, thickness of one period  $L = 20$  nm with Si and Cu layer both 10 nm: (a) two periods,  $X = x/2L$ ; (b) representative structure of superlattice with infinity periods,  $X = x/L$ .

semiconductors at both sides, the energy transfer between electrons and phonons happens twice. The length for energy exchange from phonons to electrons or from electrons to phonons is almost half of that of the aforementioned left-most metal layer. Therefore, due to the constraint of thickness, the energy exchange between electrons and phonons is weakened so that the heat flux carried by electrons is suppressed.

For metal/semiconductor super-lattice with infinity periods, the metal layer contacts with semiconductors at both sides. Correspondingly, the heat flux carried by electrons is further suppressed and thus the dominant role of electrons is further weakened, compared to bilayer films in contact with semiconductors only one side. Thus, the metal layer thickness that shows the role of electrons significant is longer. In other words, this critical thickness for considering e-ph coupling transport is longer. Fig. 10 exactly demonstrates this point. It shows the obtained thermal conductivity with and without e-ph coupling transport and the relative error between each other. These results hold the Si layer thickness constant at 10 nm and 50 nm, respectively, while varying the metal layer thickness. For metal/semiconductor super-lattice with infinity periods, if we want to control the relative error between with

and without e-ph coupling transport within 10%, it gives a critical thickness of the metal layer, i.e. 25 nm, 19 nm and 6 nm in Au/Si, Cu/Si and Al/Si super-lattice, respectively, as shown in Fig. 10. When the thickness of the metal layer is larger than the corresponding critical thickness, the e-ph coupling transport in metal layer should be considered. Otherwise, the electron heat conduction is greatly suppressed, which can be neglected for convenience, so that only phonon conduction is simulated. Besides, this critical thickness in super-lattice is nearly double that in bilayer films. As for super-lattice with infinity periods, the metal layer contacts with semiconductors at both sides in which the energy exchange between electrons and phonons happen twice. Thus, the thickness of this metal layer should be twice, so as to achieve the amount of energy transfer numerically equivalent to that in bilayer films. Therefore, if we accept the same relative error for both cases, the critical thickness of the metal layer in super-lattice is about twice that in bilayer films. Generally, within 10% error, if only one side of the metal layer contacts with semiconductors, the critical thickness of this metal layer is 12.5 nm, 7.5 nm and 2 nm for Au/Si, Cu/Si and Al/Si separately. If the metal layer contacts with semiconductors at both sides, the critical thickness is almost double, i.e. 25 nm,

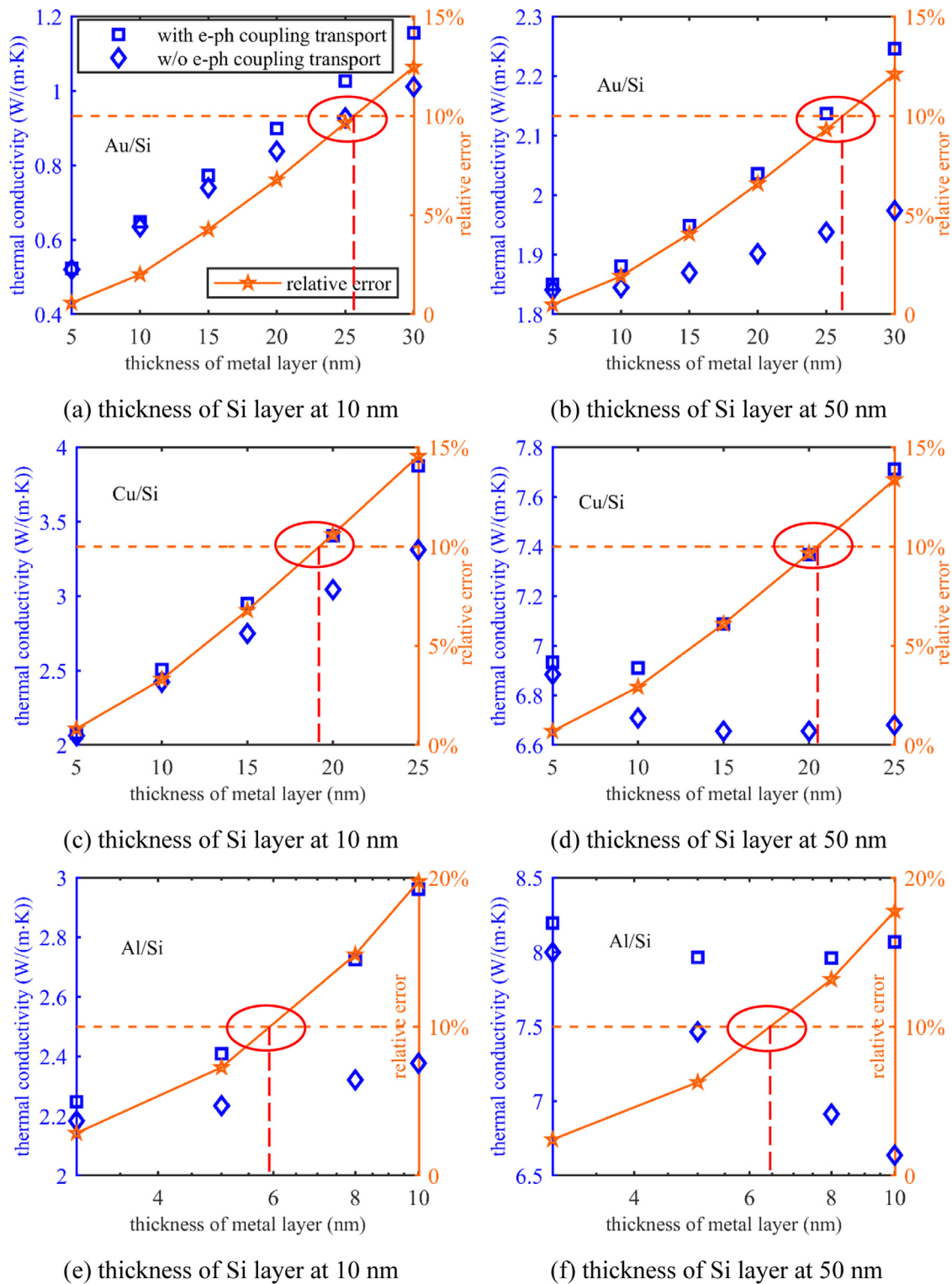


**Fig. 10.** Overall thermal conductivity of metal/semiconductor superlattice with infinity periods: (a) Au/Si, (c) Cu/Si, (e) Al/Si by keeping thickness of Si layer at 10 nm; (b) Au/Si, (d) Cu/Si, (f) Al/Si by keeping thickness of Si layer at 50 nm. The blue squares and diamonds denote the overall thermal conductivity with and without e-ph coupling transport, respectively. The orange marks represent the relative error between each other.

19 nm and 6 nm for Au/Si, Cu/Si and Al/Si, respectively. Overall, it depends on whether one side or two sides of the metal layer is in contact with semiconductors, the critical thickness is thus given. These results are in consistent with previous researches that electron heat conduction is greatly suppressed when the thickness

of the metal layer is thin enough in metal/semiconductor multilayer films or polymer/metal/polymer sandwich structure [48,54]. The present work provides an indication on whether considering e-ph coupling transport in metal/semiconductor multilayer films.

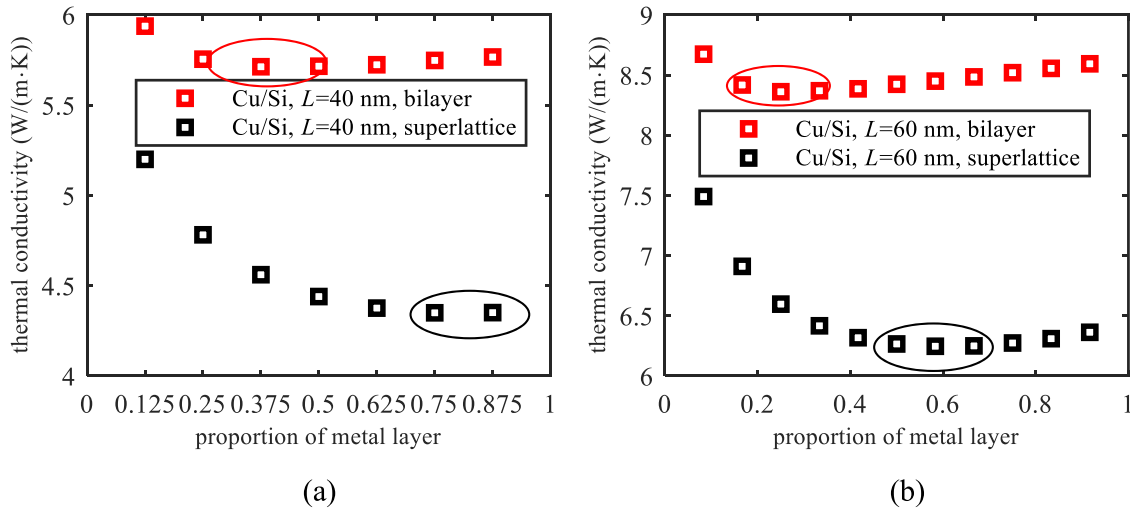


**Fig. 11.** Thermal conductivity of Cu/Si multilayer films changing with proportion of metal layer, keeping the thickness of one period constant: (a)  $L = 40$  nm; (b)  $L = 60$  nm; the red and black squares represent the thermal conductivity of bilayer and super-lattice, respectively.

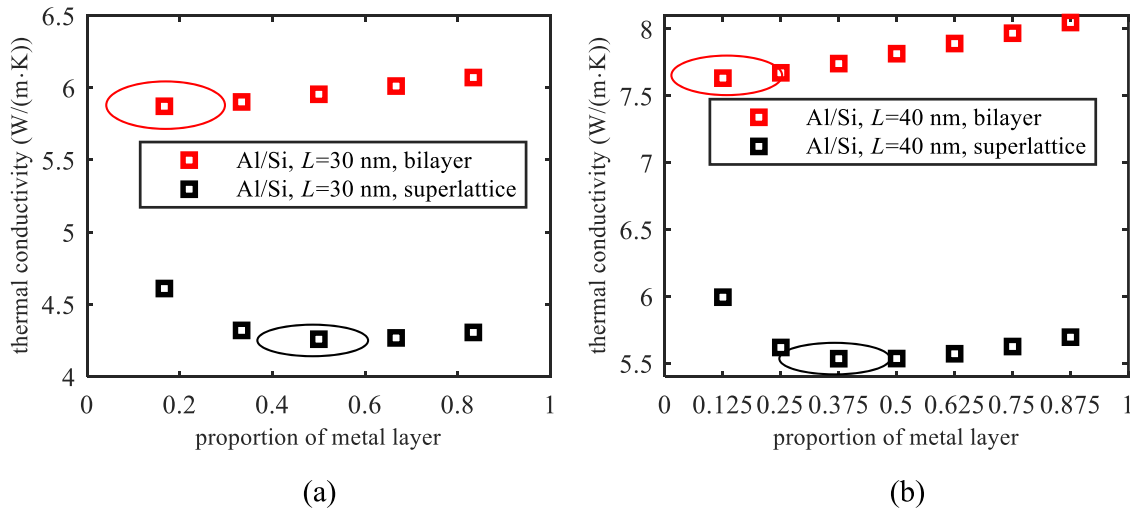


**Fig. 12.** Thermal conductivity of Al/Si multilayer films changing with proportion of metal layer, keeping the thickness of one period constant: (a)  $L = 30$  nm; (b)  $L = 40$  nm; the red and black squares represent the thermal conductivity of bilayer and super-lattice, respectively.

### 3.3. Minimum thermal conductivity

If maintain the thickness of one period constant and change the metal layer thickness, we calculate the thermal conductivity in this sub-section. We consider two cases: one is for bilayer film with one period; the other is for super-lattice with infinity periods. The results of Cu/Si, Al/Si and Au/Si multilayer films are displayed in Figs. 11, 12 and 13 separately. It shows that the thermal conductivity of bilayer films is generally larger than that of superlattice. As for superlattice, both sides of the metal layer contacts with semiconductors so that the heat flux carried by electrons is further suppressed due to the non-equilibrium between electrons and phonons at both sides. Thus, the thermal conductivity of superlattice with infinity periods is lower. Besides, for multilayer films with finite periods, its thermal conductivity lies in between the result of one period and infinity periods. With increasing the number of periods, the number of metal layers that contact with semiconductors at both sides increases and thus the thermal conductivity decreases.

These figures also show that there exists a minimum thermal conductivity in multilayers if changing the metal layer thickness. For bilayer film of one period, the thermal conductivity reaches

minimum when the metal layer thickness is at 15 nm, 5 nm, 25 nm for Cu/Si, Al/Si and Au/Si, respectively. For super-lattice with infinity periods, the minimum thermal conductivity is obtained when the metal layer thickness is at 35 nm, 12 nm, 50 nm for Cu/Si, Al/Si and Au/Si, separately. Specifically, when increasing the metal layer thickness, the length for e-ph scattering increases. The energy exchange between electrons and phonons enhances and thus the dominant role of electron heat conduction in the metal layer is improved. In contrast, while reducing the semiconductor layer thickness simultaneously, keeping the total thickness unchanged, the phonon heat conduction in the semiconductor layer is weakened by the boundary. These two effects are constrained by each other so that the thermal conductivity occurs the minimum. Additionally, the thickness corresponding to the minimum thermal conductivity for super-lattice is nearly double that for bilayer films. This relationship is similar to that whether considering e-ph coupling transport in the metal layer in Section 3.2. If the metal layer contacts with semiconductors at both sides, a thicker metal layer can achieve a certain amount of energy transfer due to the non-equilibrium between electrons and phonons at both sides. Thus, this relationship in thickness exist. Besides, for super-lattice with infinity periods, the metal layer thickness at the

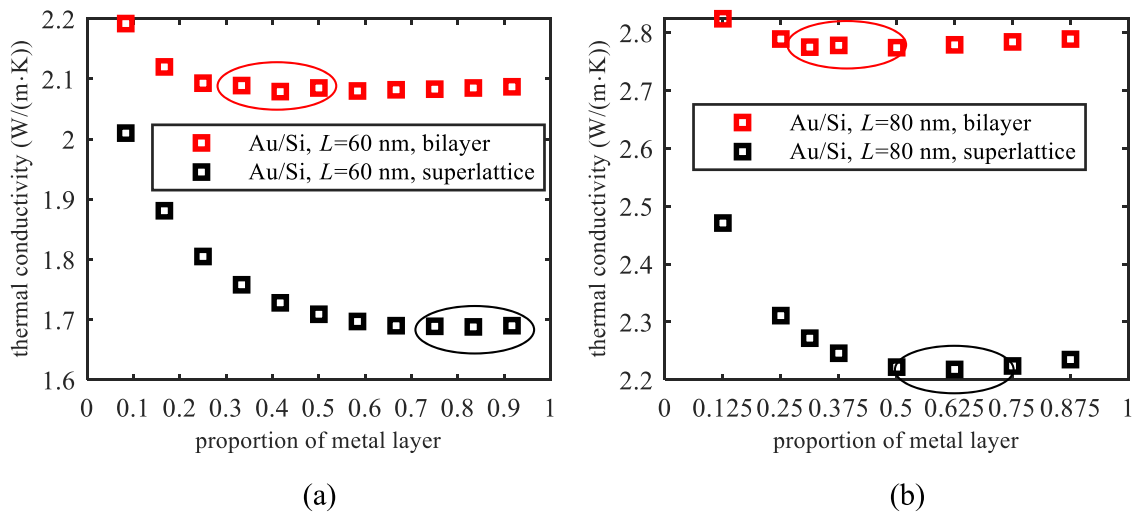


**Fig. 13.** Thermal conductivity of Au/Si multilayer films changing with proportion of metal layer, keeping the thickness of one period constant: (a)  $L = 60$  nm; (b)  $L = 80$  nm; the red and black squares represent the thermal conductivity of bilayer and super-lattice, respectively.

minimum thermal conductivity might be related to the mean free path of electrons by e-ph scattering. This mean free path calculated by Eq. (9) is about 35 nm, 18 nm and 37.5 nm for Cu, Al and Au, respectively. Correspondingly, the metal layer thickness at the minimum thermal conductivity in super-lattice is around 35 nm, 12 nm and 50 nm. When the thermal boundary resistance predicted by DMM is large, such as Au/Si, a thicker metal layer might be required to show the heat transport in the layer itself. Thus, the metal layer thickness at the minimum thermal conductivity is a little larger for Au/Si, compared to the mean free path of electrons. For the thickness studied in this Section, the minimum is 5 nm so that the wave-like or coherent effect is not discussed as a first step.

These results indicate that the addition of thin metallic layers into the thermoelectric multilayer materials might enhance its figure of merit by increasing the electric conductivity without influencing the thermal conductivity significantly. Previous works have demonstrated an improved thermoelectric power factor (the product of the electric conductivity and Seebeck coefficient squared) in metal-based super-lattice [7]. Then combined with the minimum thermal conductivity, the figure of merit will be further improved. These results will also provide the insightful indication for the manipulation of thermal conductivity in multilayers. Nevertheless, if we set that the metal layer thickness can be decreased at most to 5 nm, the magnitude of variation in thermal conductivity of the bilayer films is small. In comparison, for super-lattice, the thermal conductivity of Cu/Si, Au/Si and Al/Si can vary by 16%, 16% and 8%, respectively, due to the change in the metal layer thickness. If further reducing the metal layer thickness that can be changed, such as less than 5 nm, the magnitude of variation in thermal conductivity increases. However, there will be wave effect when the film is thin enough [55]. These results show that we can manipulate the thermal conductivity of multilayer films by changing the metal layer thickness if holding the thickness of one period constant. This manipulation strategy is more obvious for Cu/Si and Au/Si in super-lattice. When the metal layer thickness is smaller than that corresponding to a minimum thermal conductivity, the thermal conductivity decreases with increasing the metal layer thickness. Once the metal layer thickness goes beyond the above value, the thermal conductivity then increases as the increase of the metal layer thickness. The magnitude of increase is smaller than that of decrease. For multilayer films with finite periods, its result lies in be-

tween that of one period and infinity periods, and approaches to that of infinity periods with increasing the number of periods. If the two constituting materials have greatly large difference in conducting heat, the minimum thermal conductivity might exist at the thinnest or thickest metal layer. In other words, the thermal conductivity varies monotonically at the focused scale.

#### 4. Conclusions

In summary, by considering the e-ph coupling transport in metal, the present work simulates the thermal transport in metal/semiconductor multilayer films, including Au/Si, Cu/Si, and Al/Si. The calculated thermal conductivity of the Au/Si multilayers with 10 periods agrees with the experimental measurements, further validating the present transport framework. The Knudsen number of electrons is nearly one order of magnitude larger than that of phonons in metal, which further supports that we can consider the phonon interaction across the metal/semiconductor interfaces by DMM as a first step. Through comparing the thermal conductivity between with and without e-ph coupling transport, we give a critical thickness of the metal layer. When the metal layer thickness is larger than this critical thickness, i.e. 12.5 nm, 7.5 nm and 2 nm for Au/Si, Cu/Si and Al/Si bilayer films, respectively, the e-ph coupling transport in the metal layer should be considered. This critical thickness is nearly doubled for super-lattice due to the non-equilibrium at both sides, as both sides of the metal layer contacts with semiconductors in comparison to bilayer films with only one side in contact with semiconductors. As for Au with the weakest e-ph coupling constant, the largest critical thickness is thus required to show the role of electron heat conduction. Besides, if maintain the thickness of one period constant and change the metal layer thickness, we can obtain a minimum thermal conductivity in multilayer films. The present work promotes a deeper understanding of the thermal transport in metal/semiconductor multilayer films at the micro- and nanoscale and the manipulation of thermal conductivity. If we want to reduce the thermal conductivity of multilayer films, two aspects can be considered: (i) from material choice, material pairs with large thermal boundary resistance predicted by DMM and the metal with low e-ph coupling constant, such as Au/Si; (ii) from structural design, such as changing the metal layer thickness.

## Declaration of Competing Interest

The authors declare that they have no known competing financial interests or personal relationships that could have appeared to influence the work reported in this paper.

## CRediT authorship contribution statement

**Wuli Miao:** Investigation, Software, Validation, Investigation, Writing – original draft. **Moran Wang:** Conceptualization, Supervision, Writing – review & editing, Project administration.

## Data availability

No data was used for the research described in the article.

## Acknowledgments

This work is financially supported by the National Natural Science Foundation of China (No. 12272207). Our simulations are run on the “Explorer 100” cluster of Tsinghua National Laboratory for Information Science and Technology. The data that support the findings of this study are available from the corresponding author upon reasonable request.

## Appendix: Boundary conditions

In dealing with periodic heat flux boundary, we assume the left and right side of the representative structure are in temperature of  $T_h$  and  $T_c$ , respectively. It is equivalent to imposing a uniform temperature gradient  $(T_h - T_c)/L$  on the representative structure. Thus, the periodic heat flux boundary for electrons in the metal layer is formulated as:

$$I_e(x = 0, \cos \theta > 0) = I_e(x = L, \cos \theta > 0) + I_e^{eq}(T_h) - I_e^{eq}(T_c) \quad (A1)$$

$$I_e(x = L, \cos \theta < 0) = I_e(x = 0, \cos \theta < 0) + I_e^{eq}(T_c) - I_e^{eq}(T_h) \quad (A2)$$

For phonons, it is:

$$\begin{aligned} \phi_{\omega,p}(x = 0, \cos \theta > 0) \\ = \phi_{\omega,p}(x = L, \cos \theta > 0) + \phi_{\omega,p}^{eq}(T_h) - \phi_{\omega,p}^{eq}(T_c) \end{aligned} \quad (A3)$$

$$\begin{aligned} \phi_{\omega,p}(x = L, \cos \theta < 0) \\ = \phi_{\omega,p}(x = 0, \cos \theta < 0) + \phi_{\omega,p}^{eq}(T_c) - \phi_{\omega,p}^{eq}(T_h) \end{aligned} \quad (A4)$$

where,  $\theta$  denotes the angle between electron or phonon velocity direction and transport direction (i.e.  $x$  direction in Fig. 7(c)).  $I_e^{eq}$  and  $\phi_{\omega,p}^{eq}$  are the corresponding equilibrium intensities at the given temperature.

Besides, for electrons and phonons in metal, the isothermal boundary is formulated as:

$$I_e(x = 0, \cos \theta > 0) = I_e^{eq}(T_h); \quad I_e(x = L, \cos \theta < 0) = I_e^{eq}(T_c) \quad (A5)$$

$$\begin{aligned} \phi_{\omega,p}(x = 0, \cos \theta > 0) \\ = \phi_{\omega,p}^{eq}(T_h); \quad \phi_{\omega,p}(x = L, \cos \theta < 0) = \phi_{\omega,p}^{eq}(T_c) \end{aligned} \quad (A6)$$

The treatment of phonons in semiconductor is similar to that in metal.

## References

- [1] J.A. Davis, R. Venkatesan, A. Kaloyeros, M. Beylansky, S.J. Souri, K. Banerjee, K.C. Saraswat, A. Rahman, R. Reif, J.D. Meindl, Interconnect limits on gigascale integration (GSI) in the 21st century, *Proc. IEEE* 89 (2001) 305–324.
- [2] L.W. Da Silva, M. Kaviani, Micro-thermoelectric cooler: interfacial effects on thermal and electrical transport, *Int. J. Heat Mass Transf.* 47 (2004) 2417–2435.
- [3] M. Mikulics, P. Kordoš, A. Fox, M. Kočan, H. Lüth, Z. Sofer, H. Hardtdegen, Efficient heat dissipation in AlGaIn/GaN heterostructure grown on silver substrate, *Appl. Mater. Today* 7 (2017) 134–137.
- [4] J. Liu, A. Goswami, K. Jiang, F. Khan, S. Kim, R. McGee, Z. Li, Z. Hu, J. Lee, T. Thundat, Direct-current triboelectricity generation by a sliding Schottky nanocontact on MoS<sub>2</sub> multilayers, *Nat. Nanotechnol.* 13 (2018) 112–116.
- [5] Z. Wu, X. Chen, E. Mu, Y. Liu, Z. Che, C. Dun, F. Sun, X. Wang, Y. Zhang, Z. Hu, Lattice strain enhances thermoelectric properties in Sb<sub>2</sub>Te<sub>3</sub>/Te heterostructure, *Adv. Electron. Mater.* 6 (2020) 1900735.
- [6] G.D. Mahan, L.M. Woods, Multilayer thermionic refrigeration, *Phys. Rev. Lett.* 80 (1998) 4016.
- [7] D. Vashaee, A. Shakouri, Improved thermoelectric power factor in metal-based superlattices, *Phys. Rev. Lett.* 92 (2004) 106103.
- [8] D.Y. Tzou, Macro-to Microscale Heat Transfer: The Lagging Behavior, John Wiley & Sons, England, 2015.
- [9] A. Majumdar, P. Reddy, Role of electron-phonon coupling in thermal conductance of metal-nonmetal interfaces, *Appl. Phys. Lett.* 84 (2004) 4768–4770.
- [10] Y. Guo, M. Wang, Phonon hydrodynamics and its applications in nanoscale heat transport, *Phys. Rep.* 595 (2015) 1–44.
- [11] D. Jou, V.A. Cimmelli, A. Sellitto, Nonlocal heat transport with phonons and electrons: application to metallic nanowires, *Int. J. Heat Mass Transf.* 55 (2012) 2338–2344.
- [12] S. Sadasivam, N. Ye, J.P. Feser, J. Charles, K. Miao, T. Kubis, T.S. Fisher, Thermal transport across metal silicide-silicon interfaces: first-principles calculations and Green's function transport simulations, *Phys. Rev. B* 95 (2017) 085310.
- [13] J. Xu, Y. Hu, X. Ruan, X. Wang, T. Feng, H. Bao, Nonequilibrium phonon transport induced by finite sizes: effect of phonon-phonon coupling, *Phys. Rev. B* 104 (2021) 104310.
- [14] R.J. Stoner, H.J. Maris, T.R. Anthony, W.F. Banholzer, Measurements of the Kapitza conductance between diamond and several metals, *Phys. Rev. Lett.* 68 (1992) 1563.
- [15] M.L. Huberman, A.W. Overhauser, Electronic Kapitza conductance at a diamond-Pb interface, *Phys. Rev. B* 50 (1994) 2865.
- [16] A.V. Sergeev, Electronic Kapitza conductance due to inelastic electron-boundary scattering, *Phys. Rev. B* 58 (1998) R10199.
- [17] G.D. Mahan, Kapitza thermal resistance between a metal and a nonmetal, *Phys. Rev. B* 79 (2009) 075408.
- [18] A. Giri, B.M. Foley, P.E. Hopkins, Influence of hot electron scattering and electron-phonon interactions on thermal boundary conductance at metal/nonmetal interfaces, *J. Heat Transf.* 136 (2014) 092401.
- [19] T. Lu, J. Zhou, T. Nakayama, R. Yang, B. Li, Interfacial thermal conductance across metal-insulator/semiconductor interfaces due to surface states, *Phys. Rev. B* 93 (2016) 085433.
- [20] Z. Tong, H. Bao, Decompose the electron and phonon thermal transport of intermetallic compounds NiAl and Ni<sub>3</sub>Al by first-principles calculations, *Int. J. Heat Mass Transf.* 117 (2018) 972–977.
- [21] W.A. Little, The transport of heat between dissimilar solids at low temperatures, *Can. J. Phys.* 37 (1959) 334–349.
- [22] E.T. Swartz, R.O. Pohl, Thermal boundary resistance, *Rev. Modern Phys.* 61 (1989) 605.
- [23] R.J. Stoner, H.J. Maris, Kapitza conductance and heat flow between solids at temperatures from 50 to 300 K, *Phys. Rev. B* 48 (1993) 16373.
- [24] H. Lyeo, D.G. Cahill, Thermal conductance of interfaces between highly dissimilar materials, *Phys. Rev. B* 73 (2006) 144301.
- [25] G.T. Hohensee, R.B. Wilson, D.G. Cahill, Thermal conductance of metal-diamond interfaces at high pressure, *Nat. Commun.* 6 (2015) 1–9.
- [26] N. Ye, J.P. Feser, S. Sadasivam, T.S. Fisher, T. Wang, C. Ni, A. Janotti, Thermal transport across metal silicide-silicon interfaces: an experimental comparison between epitaxial and nonepitaxial interfaces, *Phys. Rev. B* 95 (2017) 085430.
- [27] Y.R. Koh, J. Shi, B. Wang, R. Hu, H. Ahmad, S. Kerdsonpanya, E. Milosevic, W.A. Doolittle, D. Gall, Z. Tian, S. Graham, P.E. Hopkins, Thermal boundary conductance across epitaxial metal/sapphire interfaces, *Phys. Rev. B* 102 (2020) 205304.
- [28] Z. Cheng, Y.R. Koh, H. Ahmad, R. Hu, J. Shi, M.E. Liao, Y. Wang, T. Bai, R. Li, E. Lee, E.A. Clinton, C.M. Matthews, Z. Engel, L. Yates, T. Luo, M.S. Goorsky, W.A. Doolittle, Z. Tian, P.E. Hopkins, S. Graham, Thermal conductance across harmonic-matched epitaxial Al-sapphire heterointerfaces, *Commun. Phys.* 3 (2020) 1–8.
- [29] J.C. Duda, C.Y.P. Yang, B.M. Foley, R. Cheaito, D.L. Medlin, R.E. Jones, P.E. Hopkins, Influence of interfacial properties on thermal transport at gold: silicon contacts, *Appl. Phys. Lett.* 102 (2013) 081902.
- [30] J. Chen, X. Xu, J. Zhou, B. Li, Interfacial thermal resistance: past, present, and future, *Rev. Modern Phys.* 94 (2022) 025002.
- [31] G. Chen, Thermal conductivity and ballistic-phonon transport in the cross-plane direction of superlattices, *Phys. Rev. B* 57 (1998) 14958.
- [32] X. Qian, X. Gu, R. Yang, Thermal conductivity modeling of hybrid organic-inorganic crystals and superlattices, *Nano Energy* 41 (2017) 394–407.
- [33] X. Ran, Y. Guo, M. Wang, Interfacial phonon transport with frequency-dependent transmissivity by Monte Carlo simulation, *Int. J. Heat Mass Transf.* 123 (2018) 616–628.
- [34] W. Bao, Z. Wang, D. Tang, Phonon transport across GaN/AlN interface: Interfacial phonon modes and phonon local non-equilibrium analysis, *Int. J. Heat Mass Transf.* 183 (2022) 122090.
- [35] Y. Wang, Z. Lu, A.K. Roy, X. Ruan, Effect of interlayer on interfacial thermal transport and hot electron cooling in metal-dielectric systems: an electron-phonon coupling perspective, *J. Appl. Phys.* 119 (2016) 065103.

- [36] Y. Wang, X. Ruan, A.K. Roy, Two-temperature nonequilibrium molecular dynamics simulation of thermal transport across metal-nonmetal interfaces, *Phys. Rev. B* 85 (2012) 205311.
- [37] Z. Lu, Y. Wang, X. Ruan, Metal/dielectric thermal interfacial transport considering cross-interface electron-phonon coupling: theory, two-temperature molecular dynamics, and thermal circuit, *Phys. Rev. B* 93 (2016) 064302.
- [38] B. Rethfeld, A. Kaiser, M. Vicanek, G. Simon, Ultrafast dynamics of nonequilibrium electrons in metals under femtosecond laser irradiation, *Phys. Rev. B* 65 (2002) 214303.
- [39] V.V. Baranov, V.V. Kabanov, Theory of electronic relaxation in a metal excited by an ultrashort optical pump, *Phys. Rev. B* 89 (2014) 125102.
- [40] B.Y. Mueller, B. Rethfeld, Relaxation dynamics in laser-excited metals under nonequilibrium conditions, *Phys. Rev. B* 87 (2013) 035139.
- [41] S. Ono, Thermalization in simple metals: role of electron-phonon and phonon-phonon scattering, *Phys. Rev. B* 97 (2018) 054310.
- [42] W. Miao, M. Wang, Nonequilibrium effects on the electron-phonon coupling constant in metals, *Phys. Rev. B* 103 (2021) 125412.
- [43] J.M. Ziman, *Electrons and Phonons: The Theory of Transport Phenomena in Solids*, Clarendon Press, Oxford, 1960.
- [44] Y. Guo, M. Wang, Heat transport in two-dimensional materials by directly solving the phonon Boltzmann equation under Callaway's dual relaxation model, *Phys. Rev. B* 96 (2017) 134312.
- [45] X. Ran, M. Wang, Efficiency improvement of discrete-ordinates method for interfacial phonon transport by Gauss-Legendre integral for frequency domain, *J. Comput. Phys.* 399 (2019) 108920.
- [46] R.M. Costescu, D.G. Cahill, F.H. Fabreguette, Z.A. Sechrist, S.M. George, Ultra-low thermal conductivity in  $W/Al_2O_3$  nanolaminates, *Science* 303 (2004) 989-990.
- [47] Y.S. Ju, M.T. Hung, M.J. Carey, M.C. Cyrille, J.R. Childress, Nanoscale heat conduction across tunnel junctions, *Appl. Phys. Lett.* 86 (2005) 203113.
- [48] Z. Li, S. Tan, E. Bozorg-Grayeli, T. Kodama, M. Asheghi, G. Delgado, M. Panzer, A. Pokrovsky, D. Wack, K.E. Goodson, Phonon dominated heat conduction normal to Mo/Si multilayers with period below 10 nm, *Nano Lett.* 12 (2012) 3121-3126.
- [49] E. Dechaumphai, D. Lu, J.J. Kan, J. Moon, E.E. Fullerton, Z. Liu, R. Chen, Ultralow thermal conductivity of multilayers with highly dissimilar debye temperatures, *Nano Lett.* 14 (2014) 2448-2455.
- [50] R. Stoner, H. Maris, Kapitza conductance and heat flow between solids at temperatures from 50 to 300 K, *Phys. Rev. B* 48 (1993) 16373.
- [51] J. Ordonez-Miranda, J.J. Alvarado-Gil, R. Yang, The effect of the electron-phonon coupling on the effective thermal conductivity of metal-nonmetal multilayers, *J. Appl. Phys.* 109 (2011) 094310.
- [52] H. Callebaut, Q. Hu, Importance of coherence for electron transport in terahertz quantum cascade lasers, *J. Appl. Phys.* 98 (2005) 104505.
- [53] J. Ravichandran, A.K. Yadav, R. Cheaito, P.B. Rossen, A. Soukiassian, S. Suresha, J.C. Duda, B.M. Foley, C.H. Lee, Y. Zhu, Crossover from incoherent to coherent phonon scattering in epitaxial oxide superlattices, *Nat. Mater.* 13 (2014) 168-172.
- [54] Z. Lu, Y. Wang, X. Ruan, The critical particle size for enhancing thermal conductivity in metal nanoparticle-polymer composites, *J. Appl. Phys.* 123 (2018) 074302.
- [55] M.N. Luckyanova, J. Garg, K. Esfarjani, A. Jandl, M.T. Bulsara, A.J. Schmidt, A.J. Minnich, S. Chen, M.S. Dresselhaus, Z. Ren, Coherent phonon heat conduction in superlattices, *Science* 338 (2012) 936-939.